Integrated PET/MR for Resting State Functional and Metabolic Imaging in Human Brain: What is Correlated and What is Impacted

Yi Shan (shanyiedu@hotmail.com)
Xuanwu Hospital, Capital Medical University https://orcid.org/0000-0003-2646-8835
Zhe Wang
Central Research Institute, United Imaging Healthcare Group, Shanghai
Shuangshuang Song
Xuanwu Hospital, Capital Medical University
Qiaoyi Xue
Central Research Institute, United Imaging Healthcare Group, Shanghai
Hongwei Yang
Xuanwu Hospital, Capital Medical Unviersity
Bixiao Cui
Xuanwu Hospital, Capital Medical University
Miao Zhang
Xuanwu Hospital, Capital Medical University
Yun Zhou
Central Research Institute, United Imaging Healthcare Group, Shanghai
Jie Lu
Xuanwu Hospital, Capital Medical University

Research Article

Keywords: PET, fMRI, Brain metabolism, Integrated PET/MR

Posted Date: July 26th, 2021

DOI: https://doi.org/10.21203/rs.3.rs-734652/v1

Abstract

Purpose

We aimed to, for the first time, investigate the interplay of simultaneous functional MRI (fMRI) and FDG PET using a randomized self-control protocol on an integrated PET/MR.

Materials and methods

24 healthy volunteers underwent PET/MR scan 30 to 40 minutes after the injection of FDG. A 22-minute brain scan was separated into MRI-off (without fMRI pulsing) and MRI-on modes (with fMRI pulsing) with each one lasting for 11 minutes. We calculated the voxel-wise fMRI metric (ReHo, ALFF, fALFF and DC), resting networks, relative standardized uptake value ratios (SUVr), Patlak Ki and regional cerebral metabolic rate of glucose (rCMRGlu) maps. Paired two-sample t-tests were applied to assess the statistical differences between SUVr, Ki, correlation coefficients of fMRI metrics and rCMRGlu between MRI-off and MRI-on mode, respectively.

Results

Voxel-wise whole brain SUVr in MRI-off mode and MRI-on mode revealed no statistical difference, while Ki was significantly elevated in the whole brain (P□0.05) during fMRI scan. Task-based group ICA revealed that the most active network components derived from combined MRI-off and MRI-on static PET images were frontal pole, superior frontal gyrus, middle temporal gyrus and occipital pole. High correlation coefficients were found among the four-fMRI metrics with rCMRGlu in MRI-off and MRI-on mode (P□0.05). The highest correlation coefficients between rCMRGlu and all fMRI metrics were found in the visual network (R, 0.523 ± 0.057) and default network (R, 0.461 ± 0.099).

Conclusions

Static PET quantitation SUVr as an indicator of the accumulative effect of FDG update post-injection does not exhibit immediate change between MRI-on and MRI-off modes. Dynamic PET quantitation Ki is instantly elevated during MRI-on mode due to the additional impact of MRI sequence on imaging subjects. Network connectivity analysis also demonstrated intermediate modulation of brain function in MRI-on mode as compared to MRI-off mode.

Introduction

PET with ^{18}F-fluorodeoxyglucose (FDG) has been regarded as the gold-standard technique to quantify brain energy metabolism. Despite standardized uptake values (SUV) reflecting regional FDG uptake, intrinsic networks derived from FDG-PET using independent-component analysis (ICA) could reflect long-

distance metabolic brain connections. Based on this data-driven technique, characteristics of the metabolic resting state networks (RSN) could be utilized to observe cognitive decline in Alzheimer's Disease and amyotrophic lateral sclerosis [1, 2]. Another promising aspect of FDG-PET is to couple glucose utilization with cerebral blood flow and oxygen consumption. Blood-oxygenation-level dependent (BOLD) functional magnetic resonance imaging (fMRI) has been commonly used to non-invasively obtain oxygen metabolism and hemodynamic response related to brain activity [3]. Neurometabolic coupling between fMRI and FDG PET metrics has provided informative biomarkers for characterizing focal differences of energy demand in a healthy population and pathology processes such as alcohol exposure and disorders of consciousness [4–6].

Integrated PET/MR system could simultaneously obtain both fMRI and FDG PET images [7, 8]. With the advantage of precisely-matched structural localization and consistent physiological states, the combined system could provide great opportunity for multiparametric analysis of interactions between brain metabolism and function [9, 10]. With the addition of FDG PET, fMRI showed potential for baseline shifts in quantifiable metabolism and neuronal signalling [11, 12]. Also, with the fusion of fMRI, FDG PET could track dynamic task-related haemodynamic and metabolic interactions with higher temporal resolution [13]. Recently, the integration of the two modalities has proved to be cost-effective for clinical research, especially in neurodegenerative disorders. Focal alterations between FDG uptake and fMRI metrics obtained by integrated PET/MR showed potential to reveal signalling hierarchies in hippocampal-cortical circuits and default mode networks in patients with Alzheimer's Disease [14–18]. Altered bioenergetic coupling across gray matter and its relationship with seizure outcomes was also reported in patients with medial temporal lobe epilepsy [19]. Thus, simultaneous PET/fMRI has become a widely adopted approach for non-invasive brain metabolic researches.

In order to shorten the time of scan, some clinical research using integrated PET/MR system prefer to run MRI sequences during the FDG uptake phase (the first 40 minutes after radiotracer administration). However, the acoustic, thermal and electromagnetic effect imposed by MRI on human brain may result in physiological inference on quantitative FDG uptake curve. Although it's been assessed on phantoms that the stability of PET quantitation was not affected during simultaneous MRI scan, even when aggressive sequence such as fast spin echo MR sequence was performed [20–22], the impact of MRI sequence pulsing was found in human studies affecting brain activation including auditory, visual and motor functional cortex [23–28]. A recent study has shown that the acoustic noise produced by fast switching gradients could cause a reproducible increase ranged from 3–9% in FDG uptake, limited to the primary auditory cortex [29]. Therefore, the timing of the fMRI scan is preferred to run during the plateau phase (30 to 40 minutes after radiotracer administration) of FDG uptake curve in clinical routine. During this period, most irreversible FDG distribution is considered to be finished with only minimal amount of free FDG in blood pool. However, few studies have proofed that the impact induced by MRI scan during this "static" period could be limited to an acceptable range in human brain. Also, whether the possible effect could influence specific metabolic parameter or neurometabolic coupling limited to focal brain cortex, network level or whole brain level, are largely unknown.

Therefore, the principal purpose of this work is to systematically evaluate the impact of simultaneous fMRI scan on quantification of brain metabolism using an integrated PET/MR system. We designed a randomized self-control study on healthy volunteers using clinically relevant imaging protocols. We will focus on the additional effect induced by fMRI sequence pulsing on voxel-wise energy consumption, spatial distribution of metabolic networks as well as the correlation between regional glucose metabolism and functional metrics within and across different resting state functional networks.

Materials And Methods

Subjects

All subjects were provided with written informed consent to undergo procedures approved by the Medical Research Ethics Committee of Xuanwu Hospital, Capital Medical University (Beijing, China). 24 healthy subjects (Male, 14, Female, 10) with ages of 31 to 66 years were enrolled in this study. Subjects were all right-handed and free of personal or family history of psychiatric or neurological disease, diabetes, renal-failure, claustrophobia and other MRI-related exclusion criteria. Prior to the scan, participants were directed to fast for at least 6 hours before the ^{18}F-FDG injection. Immediately before the scanning began, all subjects underwent a blood glucose level measurement and all measured values were below 8 mmol/L.

Data Acquisition Protocol

Simultaneous ^{18}F-FDG PET/MR scanning was performed on an integrated PET/MR system (uPMR 790, United-Imaging Healthcare, Shanghai) equipped with a 24-channel phase-array head coil [20]. Phantom experiments were initially performed to evaluate the hardware-related effects, the SUV and MRI signal stability of this integrated system (See Supplementary Materials). The MRI and PET list mode data were simultaneously acquired 30 to 40 minutes after the injection of ^{18}F-FDG as illustrated in Fig. 1.

The MRI scan started with 5 minutes of scanning for attenuation correction and 3D anatomical localization followed by a 22-minute experimental scan. Specifically, the first 5 minutes of MRI scanning consisted of a localizer and an ultra-short echo time MRI sequence for PET attenuation correction, and a three-dimensional T1 weighted fast-spoiled gradient echo sequence (voxel sizes = 1.0×1.0×1.0 mm3) for brain segmentation. The following 22-minute experimental scan was separated into MRI-off and MRI-on modes with each one lasting for 11 minutes. In the MRI-off mode, no MRI sequence was performed. In the MRI-on mode, a gradient-echo echo-planar pulse sequence (repetition time = 3000 milliseconds, echo time = 30 milliseconds, flip angle = 90°, number of slices = 43, voxel sizes = 3.0×3.0×3.0 mm3, matrix size = 64×64) was performed for resting-state BOLD-fMRI measurements lasting for 10 minutes. In order to fairly evaluate the impact of BOLD-fMRI on FDG-PET, all subjects were divided randomly in to one of two groups, who received either protocol A or B. For the protocol A group, the MRI-off mode was performed ahead of the resting-fMRI, while for the protocol B group, the scan order was reversed (see Fig. 1).

The PET list mode data had a 511KeV energy drift correction applied to correct the temperature induced counting loss during MRI scanning [22]. Dynamic data was reconstructed to 10 PET image frames (2 minutes per frame, matrix size = 192×192, field of view (FOV) = 35 cm, voxel size = 1.82×1.82×2.78 mm3) using the ordered subset-expectation maximization (OSEM) algorithm (3 iterations and 20 subsets with time-of-flight (TOF) and point-spread function (PSF)). Corrections were applied for random coincidences, dead-time, scatter and attenuation. Static data was reconstructed using all list mode events obtained during the 22-minute experimental scan (matrix size = 256 × 256, FOV = 25 cm, slice thickness = 1.4 mm, OSEM 3 iterations and 20 subsets with TOF and PSF). Whole body clinical PET/MR scan was performed after the brain scan and the SUV from aorta was used as the reference to normalize blood pool signal in Patlak Ki calculation [30].

Data Processing

Data Processing for Functional Maps

Post processing for PET and MRI images is summarized in Fig. 2. PET and MRI images were registered and jointly processed using SPM12 (Statistical Parametric Mapping, https://www.fil.ion.ucl.ac.uk/spm/software/spm12/).

Generation of Resting-State Functional Metrics from BOLD-fMRI

The pre-processing of resting-fMRI was performed using the Data Processing and Analysis for Brain Image (DPABI) tool (http://www.rfmri.org/dpabi) [31]. After slice timing correction, the alignment correction was applied to reduce the impact of head motion. FMRI images were spatially transformed to the characteristic T1-weighted structural template. The transformed fMRI images were resampled to 3 × 3 × 3 mm3, and nuisance covariates (24 head motion parameters, cerebrospinal fluid signal, white matter signal and linear trend) were regressed out. Voxel wise fMRI metric maps were generated, including regional homogeneity (ReHo), amplitude of low frequency fluctuations (ALFF), fractional amplitude of low frequency fluctuations (fALFF) and degree centrality (DC), using the DPARSF package inside DPABI. Eight resting-state networks (including visual, default, dorsal attention, auditory, ventral attention, control, sensorimotor and limbic network) were generated from the same corrected fMRI images using a group ICA analysis package (https://www.nitrc.org/projects/gift) and were used to mask out the regions of interest (ROI).

Calculation of Parametric Images from FDG-PET

After normalization of focal FDG uptake for body weight and injected dose, the relative standardized uptake value ratios (SUVr) with reference to cerebellum and white matter were calculated respectively. To quantify the change of SUVr during the time course of MRI-on and MRI-off mode acquisitions, Patlak Ki was derived from 2 min time frame brain PET image using a population-based input function and normalization factor from the aorta SUV of whole-body PET image. Analysis of the relative cerebral

metabolic rate of glucose (rCMRGlu) at each voxel was performed [32]. To allow consistent dynamic analysis, all PET dynamic images were aligned to the first time-point image and co-registered to the corresponding T1-weighted image. The voxel-wise Spearman correlation coefficient (R) between rCMRGlu and fMRI metrics was calculated using the python package Scipy (https://pypi.org/project/scipy/).

ICA Analysis for FDG-PET

Spatial ICA of the pre-processed PET images was performed within the MRI-off and MRI-on subgroups separately using the GIFT toolbox (http://mialab.mrn.org/software/). The optimal number of components of the principal component analysis was set to five which was estimated using the GIFT dimensionality estimation tool. Group ICA was used to derive task-based regional activation treating MRI-on mode as a paradigm. First, the mixing matrix was estimated, which has a unique partition for each object. The component graph of each task was calculated by projecting a single task data onto the inverse of the mixing matrix partition. Task-specific time courses and images were used to make group and inter-group inferences [33]. Each spatial map was converted to Z-values and activation maps were visualized using binary masks generated with a threshold of 1.5.

Statistical Analysis

Statistical analysis was performed using DPABI and Statistical Product and Service Solutions (IBM SPSS version 20). Paired two-sample t-tests were applied to assess the significance of SUV, SUVr, Ki of Patlak model between MRI-off and MRI-on mode, respectively. The voxel-wise paired t-test between whole brain SUVr in MRI-off mode and MRI-on mode was performed using DPABI. Comparisons within correlation coefficients of functional metrics (ReHo, ALFF, fALFF and DC) and rCMRGlu among the eight networks between MRI-on mode and MRI-off mode were calculated with one-way ANOVA analysis and paired two-sample t-test, respectively.

Results

MRI Impact on FDG Uptake

Phantom results have verified the system stability for simultaneous PET/fMRI acquisition (Fig. S1 and Table S1). Static PET images from MRI-off and MRI-on mode produced similar SUVr(SUV_{WB}/SUV_{CB})distribution maps (Fig. 3A and 3B). From visual inspection, concordant distributions were found without focal areas of abnormal hyper- or hypo- metabolism. Voxel-wise paired t-tests between whole brain SUVr in MRI-off mode and MRI-on mode revealed no statistical difference (P ≥ 0.05), while Patlak Ki significantly increased when comparing MRI-on mode with MRI-off mode (P≤0.001, Fig. 3C and 3D). Mean SUVr and Patlak Ki values for whole brain (WB) and different anatomical structure including grey matter (GM), white matter (WM), cerebellum (CB) and eight functional networks were calculated (Fig. 4). Mean Patlak Ki significantly increased when comparing MRI-on mode with MRI-off mode, while mean SUVr showed no statistical difference (P ≥ 0.05). The same measurement using white matter as a reference tissue was performed and a similar result was confirmed (Fig. S2).

MRI Impact on Metabolic Network

The most active network components derived from PET static spatial ICA were located in the auditory, default, visual and language networks (Fig. 5A and 5B). From visual inspection, there was little difference observed between the component maps calculated from PET image generated during MRI-off and MRI-on mode. Group ICA which treated fMRI scan as a stimulating paradigm revealed that the most active network components were frontal pole, superior frontal gyrus, middle temporal gyrus and occipital pole (Fig. 5C).

Impact of Simultaneous Scan on Neurometabolic Coupling

Spatial correlation maps between rCMRGlu and four fMRI metrics, as well as the results of the correlation analysis over each of the eight resting-state networks are shown in Fig. 6. Overall, high correlation coefficients were found among the four-fMRI metrics with rCMRGlu in MRI-off and MRI-on mode (mean R for ALFF, fALFF, DC and ReHo, 0.195 ± 0.260, 0.296 ± 0.180, 0.287 ± 0.164, 0.413 ± 0.145, P = 0.022). ReHo provided significantly higher correlation coefficients with rCMRGlu, compared to other metrics (ReHo and ALFF, P = 0.013, ReHo and fALFF, P□0.001, ReHo and DC, P = 0.002). No difference was found between other metrics (ALFF and fALFF, P = 0.144, fALFF and DC, P = 0.686, ALFF and DC, P = 0.080). The highest correlation coefficients between rCMRGlu and all fMRI metrics were found in the visual network (mean R, 0.523 ± 0.057) and default network (mean R, 0.461 ± 0.099).

Discussion

To the best of our knowledge, this work is the first study systematically assessing the impact of simultaneous fMRI scan on FDG-PET in human brain with an integrated PET/MR system. Our protocol is a self-control study design following the recommended clinical routine, where MR sequences were performed 30 to 40 minutes after the injection of ^{18}F-FDG. It's commonly considered that FDG-PET data acquired during this plateau phase of uptake curve mainly represents the neuronal activity occurred during the preceding early uptake phase. Thus, SUVr for plateau phase is supposed to be steady even when fMRI scan is synchronously performed. Our results found no difference in neither mean SUVr nor voxel-wise SUVr compared between MRI-on and MRI-off period, which supported this inference. However, obvious increase of Patlak Ki was detected in MRI-on period across the whole brain, including grey matter, white matter, cerebellum and eight specific functional networks. This unspecific global metabolic change reflects a short-term FDG uptake elevation due to the fMRI scan, but may not in favour of a neuronal origin, whose activation should mainly locate in grey matter regions. We assume that this phenomenon may due to other physiological inference, such as temperature-dependent acceleration of metabolic rates. Thus, with only minor amount of free FDG in blood pool available, fMRI scan in the steady state could only produce limited and unspecific effect on the trend of FDG elevation, which does not affect the calculation of SUVr value to statistical significance.

In the network-wise comparison, when treating fMRI scan as a stimulation task, the effected components were located in the default, auditory, visual and language networks, which were commonly regarded as “higher-order” cognitive networks. A previous study reported that 13 meaningful RSNs could be detected from FDG-PET data acquired 10 minutes to 30 minutes post-injection. Among them, seven networks could be detected by both modalities, including default mode, left central executive, primary and secondary visual, sensorimotor, cerebellar, and auditory networks [34]. In our study, the “activated” networks induced by fMRI scan fundamentally located in these “dually” detected RSNs, which could be explained by changes of either cerebral blood flow or activity-dependent glucose consumption. As our data was acquired 30 minutes post-injection, the contribution of a blood flow signal change caused by the instant injection of FDG could be negligible. In this way, these “activations” observed in our ICA results should be regarded as comparable elevated glucose consumption, rather than increased cerebral blood flow or oxygen consumption.

In previous studies, the possible mechanism underlying neurometabolic coupling was explained by temporally synchronized cerebral blood flow and energy utilization, based on the theory that resting-state glucose and oxygen metabolism were closely linked [35]. Strong coupling was found in default and visual networks, while weak correlation was found in limbic and somatomotor network [36]. The highest correlation between rCMRGlu and fMRI metrics were achieved in ReHo, which was both detected by using integrated PET/MR or separated PET and MRI devices [3, 36, 37]. Other metrics, such as ALFF or DC, showed lower association with CMRGlu, maybe strongly affected by venous vasculature or other non-neuronal factors on signal amplitude [3]. These differences could also be explained by the different physiological phenomena probed by each metric. ALFF contrast is only due to single voxel signal. ReHo could be considered as a measurement of short-range FC affected by neighbouring 27 voxels, while DC measures distant voxels weighted by long-range FC in the whole brain.

Our study reports a synthesis effect of MRI scan on quantitative PET in an integrated system. Among all possible factors, acoustic MRI noise resulting from echo-planar imaging (EPI) should be regarded as the main concern. This sequence is normally accompanied by a gradient-shifting noise with sound level greater than 100dB [28]. Studies have focused on measuring how background acoustic noise influence the hemodynamic responses in auditory cortex and made efforts to spoil the interference [24]. Reduced activation in the visual cortex was also reported, which may relate to attention modulation due to auditory-visual cross-modal neural interaction [28]. Increased activation of working-memory network [27], as well as suppressed activation in the default-mode network and sensorimotor cortex [25, 26], were respectively discussed under the presence of BOLD-related noise. “Quieter” fMRI acquisition methods, such as sparse temporal sampling or interleaved silent steady state, could be applied to a less noisy background environment for BOLD-fMRI scan [23]. In addition, MR-induced RF power deposition and the resulting effects on temperature-dependent metabolic rates could also influence FDG uptake, with maximum relative increases of 26% for uptake models based on metabolism [38]. We speculate that these above factors synergistically influenced brain metabolism during the static phase of FDG uptake in our study.

This work was subject to several limitations. First, we adopted a blood-free approach to estimate the relative quantification of CMRGlu, which is more tolerable for a universal clinical routine. However, for a more precise design, absolute quantification of CMRGlu could be calculated by infusion of ^{18}F-FDG and venous blood sampling [39]. Second, methodologically, ICA and seed-based functional connectivity (sbFC) are two main approaches for statistical mapping of RSNs derived from FDG-PET. It's been discussed that the choice of ICA or sbFC could influence the detectability of RSNs especially when sample size is limited [40]. Future studies could retest and verify our results by different data analysis methods on the basis of a larger dataset.

Declarations

Acknowledgements

We thank Dr. Adam Chandler for proof-reading and language polishing. We thank Dr. Hui Liu and Dr. Jian-min Yuan for analysing and interpreting the data. We thank Dr. Ling-zhi Hu for enhancing intellectual content and providing instrumental discussion to our manuscript.

Compliance with Ethical Standards

This work was supported by the National Key Research and Development Program of China (Grant No. 2016YFC0103909), the National Natural Science Foundation of China (Grant No. 81671662) and the Beijing Municipal Administration of Hospitals' Ascent Plan (Grant No. DFL20180802).

All authors declare no conflict of interest.

All procedures performed in studies involving human participants were in accordance with the ethical standards of the committee of Xuanwu Hospital, Capital Medical University, and with the 1964 Helsinki declaration and its later amendments or comparable ethical standards. Informed consent was obtained from all individual participants included in the study.

References

1. Pagani M, Giuliani A, Oberg J, De Carli F, Morbelli S, Girtler N, et al. Progressive Disintegration of Brain Networking from Normal Aging to Alzheimer Disease: Analysis of Independent Components of (18)F-FDG PET Data. J Nucl Med. 2017;58:1132–9. doi:10.2967/jnumed.116.184309.
2. Pagani M, Oberg J, De Carli F, Calvo A, Moglia C, Canosa A, et al. Metabolic spatial connectivity in amyotrophic lateral sclerosis as revealed by independent component analysis. Hum Brain Mapp. 2016;37:942–53. doi:10.1002/hbm.23078.
3. Bernier M, Croteau E, Castellano CA, Cunnane SC, Whittingstall K. Spatial distribution of resting-state BOLD regional homogeneity as a predictor of brain glucose uptake: A study in healthy aging. NeuroImage. 2017;150:14–22. doi:10.1016/j.neuroimage.2017.01.055.

4. Shokri-Kojori E, Tomasi D, Alipanahi B, Wiers CE, Wang GJ, Volkow ND. Correspondence between cerebral glucose metabolism and BOLD reveals relative power and cost in human brain. Nat Commun. 2019;10:690. doi:10.1038/s41467-019-08546-x.
5. Soddu A, Gomez F, Heine L, Di Perri C, Bahri MA, Voss HU, et al. Correlation between resting state fMRI total neuronal activity and PET metabolism in healthy controls and patients with disorders of consciousness. Brain Behav. 2016;6:e00424. doi:10.1002/brb3.424.
6. Tomasi DG, Shokri-Kojori E, Wiers CE, Kim SW, Demiral SB, Cabrera EA, et al. Dynamic brain glucose metabolism identifies anti-correlated cortical-cerebellar networks at rest. J Cereb Blood Flow Metab. 2017;37:3659–70. doi:10.1177/0271678X17708692.
7. Chen Z, Jamadar SD, Li S, Sforazzini F, Baran J, Ferris N, et al. From simultaneous to synergistic MR-PET brain imaging: A review of hybrid MR-PET imaging methodologies. Hum Brain Mapp. 2018;39:5126–44. doi:10.1002/hbm.24314.
8. Disselhorst JA, Bezrukov I, Kolb A, Parl C, Pichler BJ. Principles of PET/MR Imaging. J Nucl Med. 2014;55:2S–10S. doi:10.2967/jnumed.113.129098.
9. Heiss WD. The potential of PET/MR for brain imaging. Eur J Nucl Med Mol Imaging. 2009;36(Suppl 1):105-12. doi:10.1007/s00259-008-0962-3.
10. Verger A, Guedj E. The renaissance of functional (18)F-FDG PET brain activation imaging. Eur J Nucl Med Mol Imaging. 2018;45:2338–41. doi:10.1007/s00259-018-4165-2.
11. Riedl V, Bienkowska K, Strobel C, Tahmasian M, Grimmer T, Forster S, et al. Local Activity Determines Functional Connectivity in the Resting Human Brain: A Simultaneous FDG-PET/fMRI Study. J Neurosci. 2014;34:6260–6. doi:10.1523/jneurosci.0492-14.2014.
12. Riedl V, Utz L, Castrillon G, Grimmer T, Rauschecker JP, Ploner M, et al. Metabolic connectivity mapping reveals effective connectivity in the resting human brain. Proc Natl Acad Sci U S A. 2016;113:428–33. doi:10.1073/pnas.1513752113.
13. Jamadar SD, Ward PG, Li S, Sforazzini F, Baran J, Chen Z, et al. Simultaneous task-based BOLD-fMRI and [18-F] FDG functional PET for measurement of neuronal metabolism in the human visual cortex. NeuroImage. 2019;189:258–66. doi:10.1016/j.neuroimage.2019.01.003.
14. Marchitelli R, Aiello M, Cachia A, Quarantelli M, Cavaliere C, Postiglione A, et al. Simultaneous resting-state FDG-PET/fMRI in Alzheimer Disease: Relationship between glucose metabolism and intrinsic activity. NeuroImage. 2018;176:246–58. doi:10.1016/j.neuroimage.2018.04.048.
15. Scherr M, Utz L, Tahmasian M, Pasquini L, Grothe MJ, Rauschecker JP, et al. Effective connectivity in the default mode network is distinctively disrupted in Alzheimer's disease-A simultaneous resting-state FDG-PET/fMRI study. Hum Brain Mapp. 2019. doi:10.1002/hbm.24517.
16. Tahmasian M, Pasquini L, Scherr M, Meng C, Förster S, Mulej Bratec S, et al. The lower hippocampus global connectivity, the higher its local metabolism in Alzheimer disease. Neurology. 2015;84:1956–63. doi:10.1212/WNL.0000000000001575.
17. Tahmasian M, Shao J, Meng C, Grimmer T, Diehl-Schmid J, Yousefi BH, et al. Based on the Network Degeneration Hypothesis: Separating Individual Patients with Different Neurodegenerative

Syndromes in a Preliminary Hybrid PET/MR Study. J Nucl Med. 2016;57:410–5. doi:10.2967/jnumed.115.165464.

18. Yan S, Zheng C, Cui B, Qi Z, Zhao Z, An Y, et al. Multiparametric imaging hippocampal neurodegeneration and functional connectivity with simultaneous PET/MRI in Alzheimer's disease. Eur J Nucl Med Mol Imaging. 2020. doi:10.1007/s00259-020-04752-8.
19. Wang J, Shan Y, Dai J, Cui B, Shang K, Yang H, et al. Altered coupling between resting-state glucose metabolism and functional activity in epilepsy. Ann Clin Transl Neurol. 2020;7:1831–42. doi:10.1002/acn3.51168.
20. Chen S, Gu Y, Yu H, Chen X, Cao T, Hu L, et al. NEMA NU2-2012 performance measurements of the United Imaging uPMR790: an integrated PET/MR system. Eur J Nucl Med Mol Imaging. 2021. doi:10.1007/s00259-020-05135-9.
21. Deller TW, Khalighi MM, Jansen FP, Glover GH. PET Imaging Stability Measurements During Simultaneous Pulsing of Aggressive MR Sequences on the SIGNA PET/MR System. J Nucl Med. 2018;59:167–72. doi:10.2967/jnumed.117.194928.
22. Grant AM, Deller TW, Khalighi MM, Maramraju SH, Delso G, Levin CS. NEMA NU 2-2012 performance studies for the SiPM-based ToF-PET component of the GE SIGNA PET/MR system. Med Phys. 2016;43:2334. doi:10.1118/1.4945416.
23. Andoh J, Ferreira M, Leppert IR, Matsushita R, Pike B, Zatorre RJ. How restful is it with all that noise? Comparison of Interleaved silent steady state (ISSS) and conventional imaging in resting-state fMRI. NeuroImage. 2017;147:726–35. doi:10.1016/j.neuroimage.2016.11.065.
24. Di Salle F, Formisano E, Seifritz E, Linden DE, Scheffler K, Saulino C, et al. Functional fields in human auditory cortex revealed by time-resolved fMRI without interference of EPI noise. NeuroImage. 2001;13:328–38. doi:10.1006/nimg.2000.0683.
25. Fuchino Y, Sato H, Maki A, Yamamoto Y, Katura T, Obata A, et al. Effect of fMRI acoustic noise on sensorimotor activation examined using optical topography. NeuroImage. 2006;32:771–7. doi:10.1016/j.neuroimage.2006.04.197.
26. Gaab N, Gabrieli JD, Glover GH. Resting in peace or noise: scanner background noise suppresses default-mode network. Hum Brain Mapp. 2008;29:858–67. doi:10.1002/hbm.20578.
27. Tomasi D, Caparelli EC, Chang L, Ernst T. fMRI-acoustic noise alters brain activation during working memory tasks. NeuroImage. 2005;27:377–86. doi:10.1016/j.neuroimage.2005.04.010.
28. Zhang N, Zhu XH, Chen W. Influence of gradient acoustic noise on fMRI response in the human visual cortex. Magnetic resonance in medicine. 2005;54:258–63. doi:10.1002/mrm.20512.
29. Chonde DB, Abolmaali N, Arabasz G, Guimaraes AR, Catana C. Effect of MRI acoustic noise on cerebral fludeoxyglucose uptake in simultaneous MR-PET imaging. Invest Radiol. 2013;48:302–12. doi:10.1097/RLI.0b013e3182839fbc.
30. Wu Y, Zhou Y, Bao S, Huang S, Zhao X, Li J. Using the rPatlak plot and dynamic FDG-PET to generate parametric images of relative local cerebral metabolic rate of glucose. Science Bulletin. 2012;57.

31. Yan CG, Wang XD, Zuo XN, Zang YF. DPABI: Data Processing & Analysis for (Resting-State). Brain Imaging Neuroinformatics. 2016;14:339–51. doi:10.1007/s12021-016-9299-4.
32. Wang Q, Kjaer T, Jorgensen MB, Paulson OB, Lassen NA, Diemer NH, et al. Nitric oxide does not act as a mediator coupling cerebral blood flow to neural activity following somatosensory stimuli in rats. Neurol Res. 1993;15:33–6. doi:10.1080/01616412.1993.11740103.
33. Calhoun VD, Liu J, Adali T. A review of group ICA for fMRI data and ICA for joint inference of imaging, genetic, and ERP data. NeuroImage. 2009;45:163-72. doi:10.1016/j.neuroimage.2008.10.057.
34. Savio A, Funger S, Tahmasian M, Rachakonda S, Manoliu A, Sorg C, et al. Resting-State Networks as Simultaneously Measured with Functional MRI and PET. J Nucl Med. 2017;58:1314–7. doi:10.2967/jnumed.116.185835.
35. Wang J, Sun H, Cui B, Yang H, Shan Y, Dong C, et al. The Relationship Among Glucose Metabolism, Cerebral Blood Flow, and Functional Activity: a Hybrid PET/fMRI Study. Mol Neurobiol. 2021;58:2862–73. doi:10.1007/s12035-021-02305-0.
36. Aiello M, Salvatore E, Cachia A, Pappata S, Cavaliere C, Prinster A, et al. Relationship between simultaneously acquired resting-state regional cerebral glucose metabolism and functional MRI: a PET/MR hybrid scanner study. NeuroImage. 2015;113:111–21. doi:10.1016/j.neuroimage.2015.03.017.
37. Jiao F, Gao Z, Shi K, Jia X, Wu P, Jiang C, et al. Frequency-Dependent Relationship Between Resting-State fMRI and Glucose Metabolism in the Elderly. Front Neurol. 2019;10:566. doi:10.3389/fneur.2019.00566.
38. Carluccio G, Ding YS, Logan J, Collins CM. On the potential for RF heating in MRI to affect metabolic rates and (18) FDG signal in PET/MR: simulations of long-duration, maximum normal mode heating. Med Phys. 2017;44:589–96. doi:10.1002/mp.12046.
39. Hahn A, Gryglewski G, Nics L, Hienert M, Rischka L, Vraka C, et al. Quantification of Task-Specific Glucose Metabolism with Constant Infusion of 18F-FDG. J Nucl Med. 2016;57:1933–40. doi:10.2967/jnumed.116.176156.
40. Trotta N, Baete K, Laere KV, Goldman S, Tiege X, Wens V. Neurometabolic Resting-State Networks Derived from Seed-Based Functional Connectivity Analysis. J Nucl Med. 2018;59:1642–3. doi:10.2967/jnumed.118.212878.

Figures

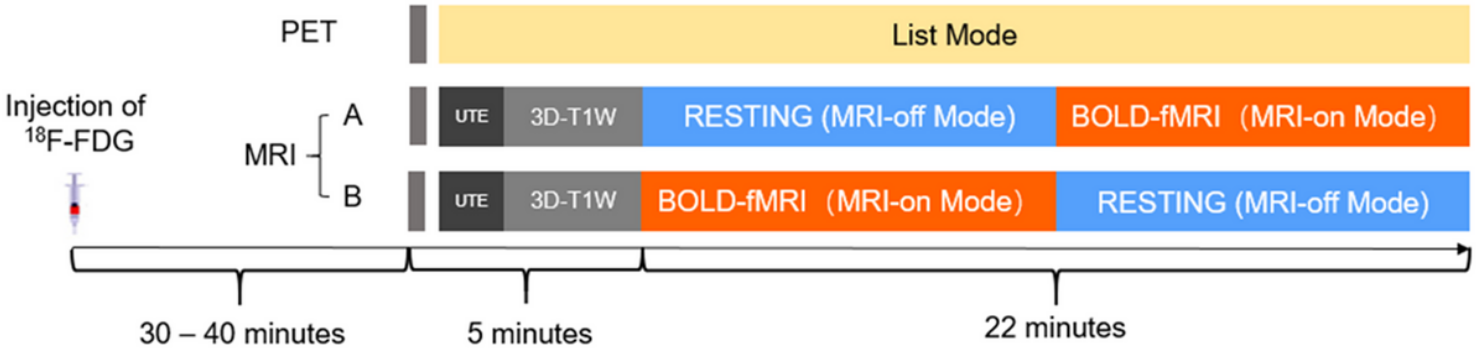

Figure 1

Schematic diagram of the simultaneous 18F-FDG PET/MR acquisition protocol. 18F-FDG - 18F-2-fluro-D-deoxy-glucose, UTE - ultra-short echo, 3D-T1W - three dimensional T1 weighted sequence.

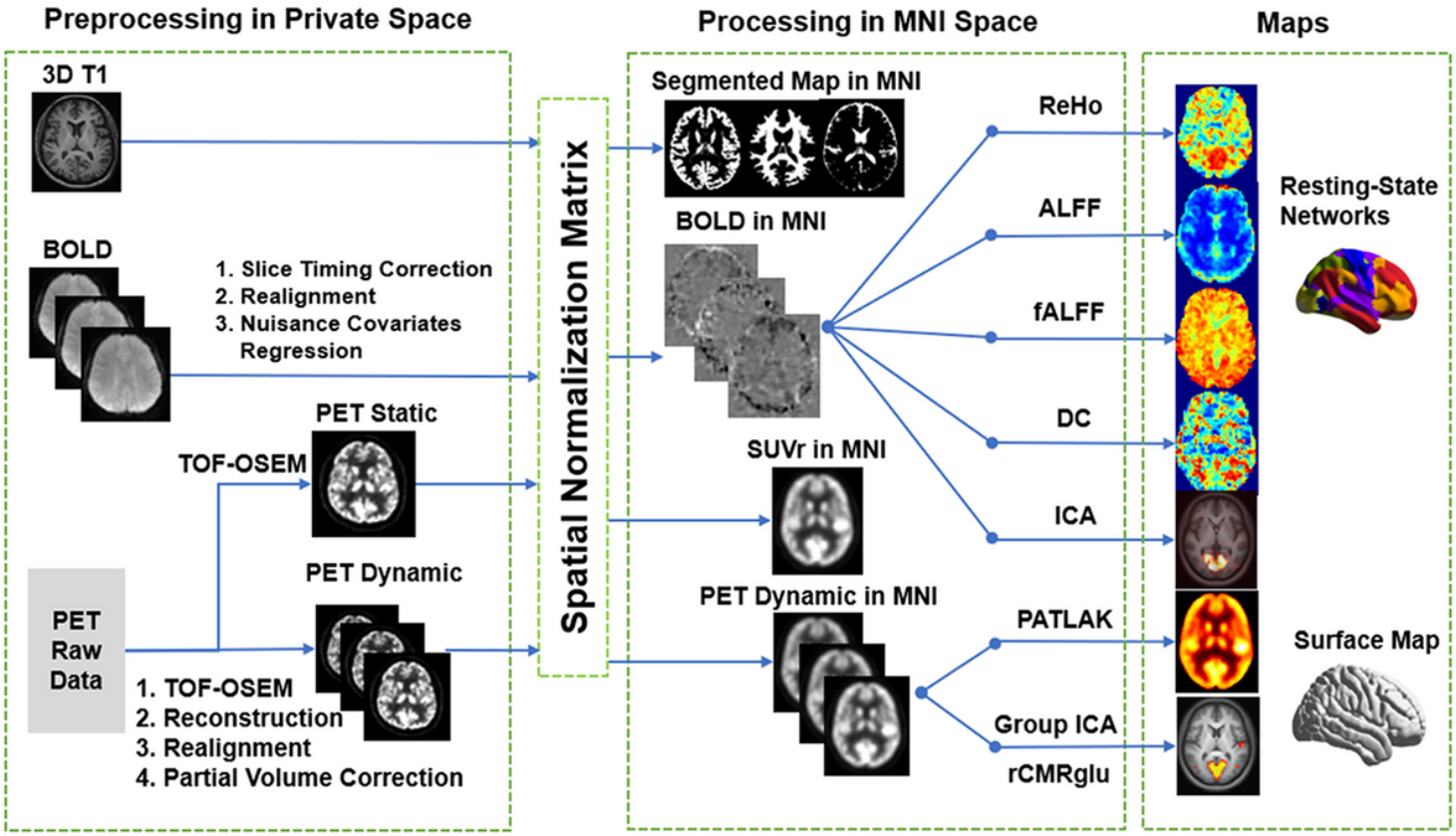

Figure 2

Schematic diagram of data processing protocol. The calculation of SUVr, fMRI metrics, metabolic networks and rCMRGlu maps were illustrated.

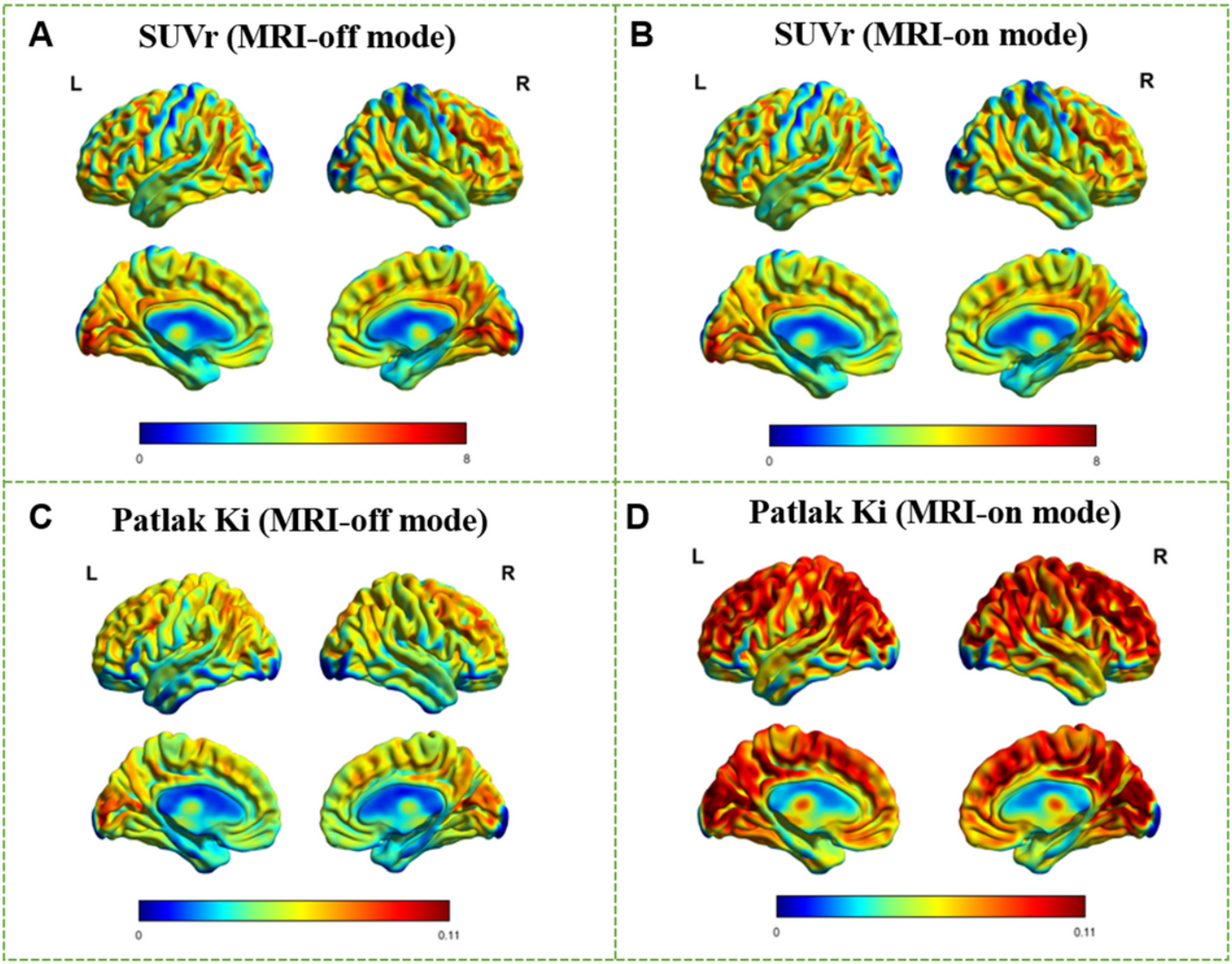

Figure 3

Voxel-wise comparison between MRI-off and MRI-on mode. SUVr and Ki in MRI-off mode (A and C) and MRI-on mode (B and D) overlaid on three orthogonal views of the brain for a randomly selected subject. Average SUVr and Ki across subjects superimposed on dorsal (top) and medial (right bottom) surface views of the cerebrum.

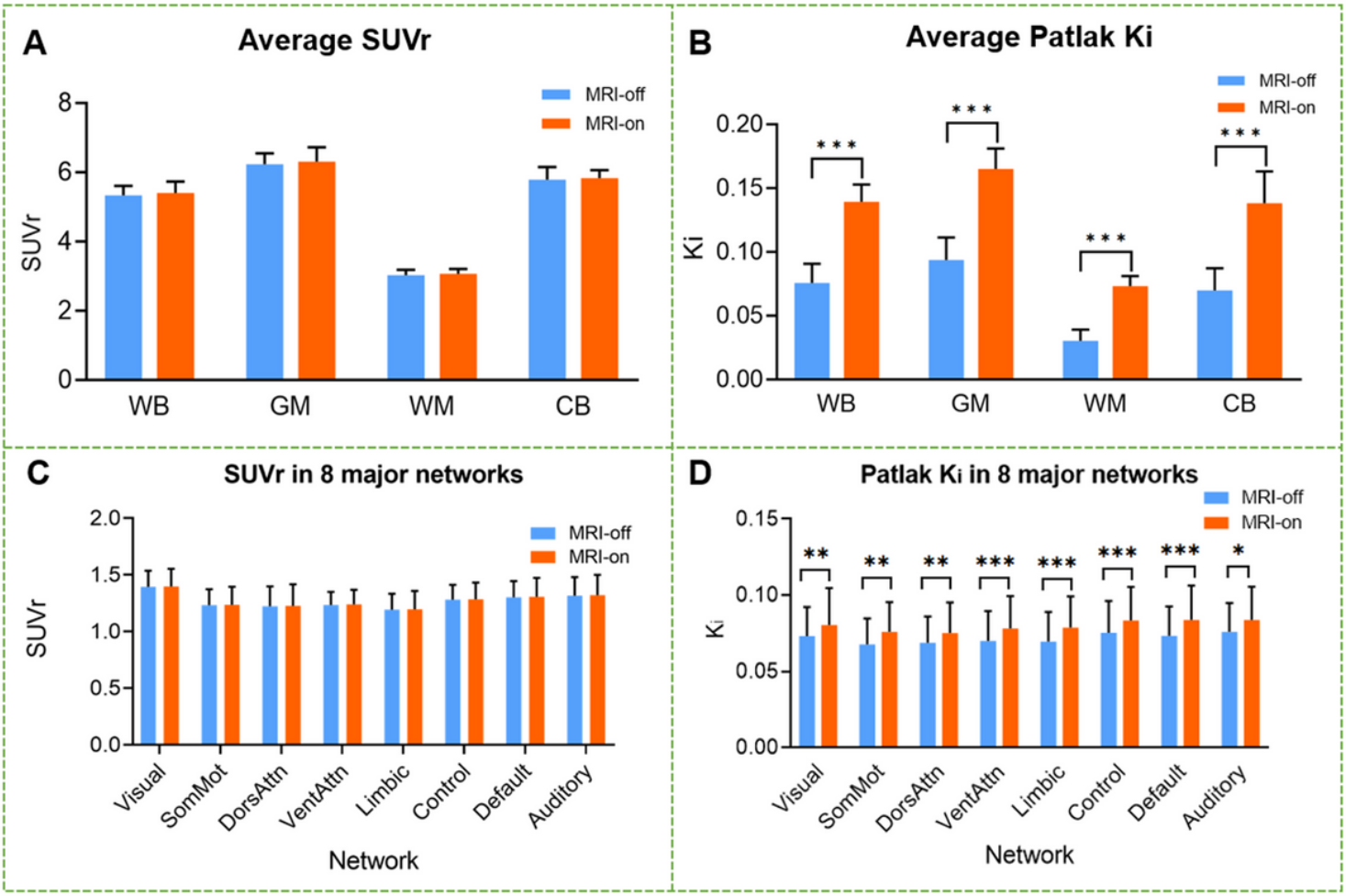

Figure 4

Comparison between average SUV and Ki in MRI-on mode and MRI-off mode. The mean of SUVr (A and C) and Ki (B and D) was compared across the whole brain (WB), grey matter (GM), white matter (WM), cerebellum (CB) and eight major networks for all the subjects scanned in MRI-off and MRI-on modes. Error bars are standard error. * P value≤0.05; ** P value≤0.01; *** P value≤0.001.

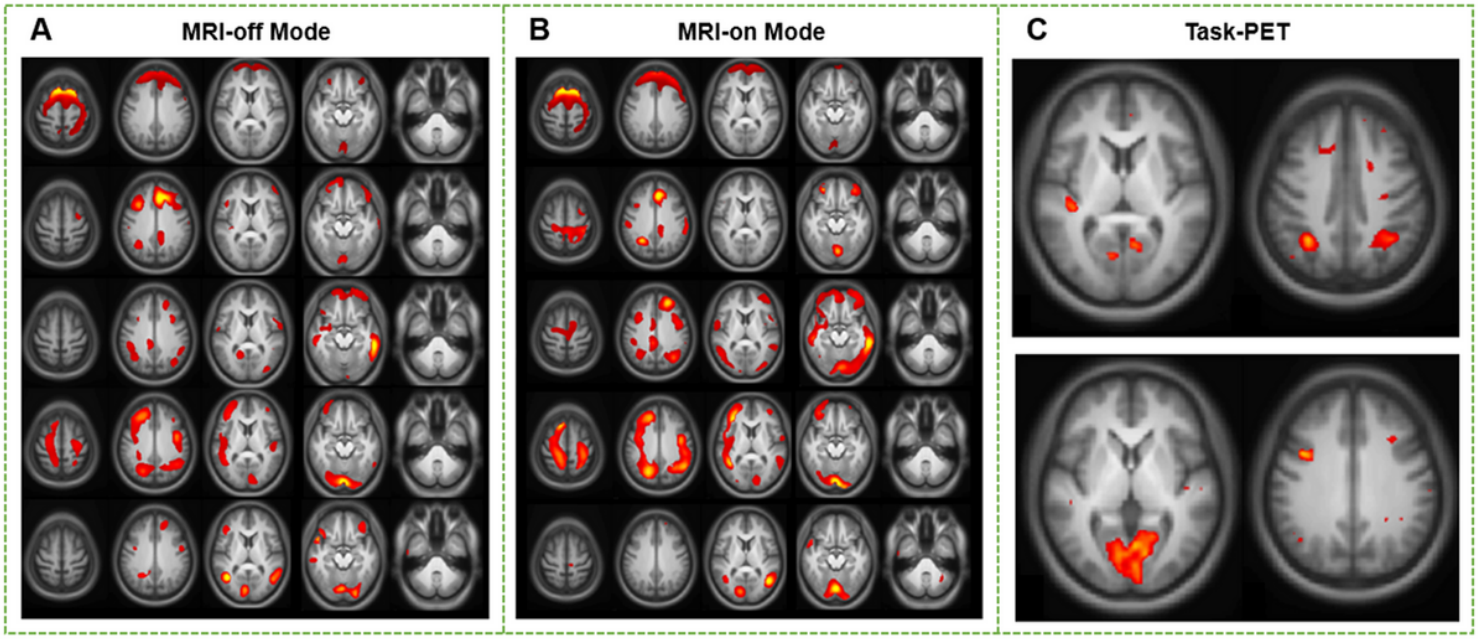

Figure 5

Comparison between static spatial ICA in MRI-off and MRI-on mode. Major networks from resting PET SUVr images in MRI-off and MRI-on mode were persevered (A and B). Network activation through group-ICA of combined MRI-off and MRI-on mode, treating fMRI noise as a stimulating paradigm (C).

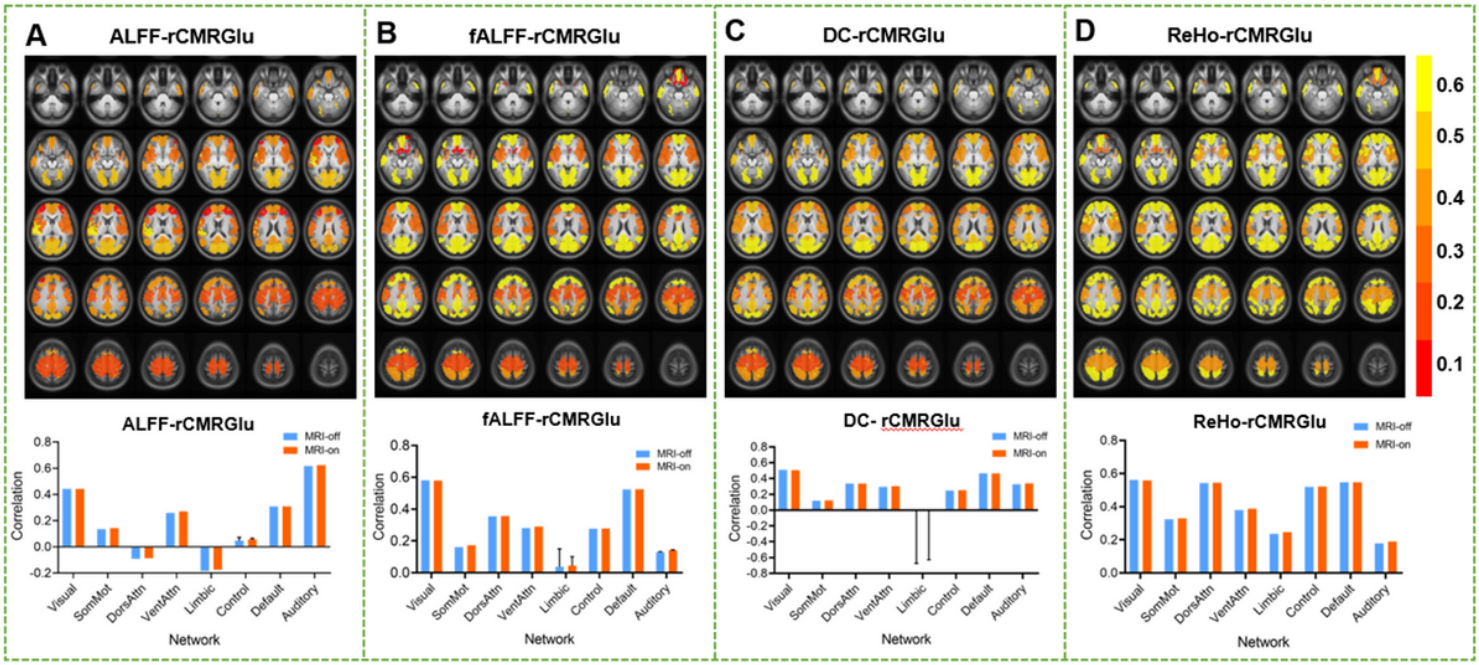

Figure 6

Spatial correlation between rCMRGlu and fMRI metrics, ALFF (A), fALFF (B), DC (C), and ReHo (D) in MRI-on mode. The comparison between the corresponding correlation statistics (averaged across all subjects) across the eight networks in the MRI-off and MRI-on mode are shown, respectively.

Supplementary Files

This is a list of supplementary files associated with this preprint. Click to download.

- SupplementaryMaterial.docx